



# Robust Posegraph Optimization Using Proximity Points

Tazaki, Yuichi

Wada, Kotaro

Nagano, Hikaru

Yokokohji, Yasuyoshi

---

## (Citation)

Journal of Robotics and Mechatronics, 35(6):1480-1488

## (Issue Date)

2023-12-20

## (Resource Type)

journal article

## (Version)

Version of Record

## (Rights)

© Fuji Technology Press Ltd.

This article is published under a Creative Commons Attribution-NoDerivatives 4.0 International License.

## (URL)

<https://hdl.handle.net/20.500.14094/0100486210>



Paper:

# Robust Posegraph Optimization Using Proximity Points

Yuichi Tazaki, Kotaro Wada, Hikaru Nagano, and Yasuyoshi Yokokohji

Graduate School of Engineering, Kobe University  
Rokkodai-cho, Nada-ku, Kobe, Hyogo 657-0013, Japan

E-mail: tazaki@mech.kobe-u.ac.jp

[Received May 30, 2023; accepted August 2, 2023]

**This paper proposes a robust posegraph optimization (PGO) method for posegraphs with keypoints. In the conventional PGO formulation, a loop constraint is defined between a pair of nodes, whereas in the proposed method, it is defined between a pair of keypoints. In this manner, robust PGO based on switch variables can be realized in a more fine-grained manner. Loop constraint is defined based on the unique geometric property of proximity point, and implemented as a new edge type of the  $g^2o$  solver. The proposed method is compared with other robust PGO methods using real world data recorded in Nakanoshima Robot Challenge 2021.**

**Keywords:** mobile robot, proximity points, robust posegraph optimization

## 1. Introduction

In recent years, rapid aging of the society and rising cost of human labor have been strongly pushing many fields of industry and service towards automation. The SLAM technology, which enables a robot to build a map of the working environment, localize itself in the map, and navigate itself in the environment, is one of the key building blocks of autonomous robots [1]. One fundamental technical issue that arises when a robot operates in a large-scale environment for a long duration of time is how to build and maintain a map in a concise and usable form.

Posegraph is a graphical map representation in which places are represented by nodes and traversability between places are expressed by edges. It is considered more suitable to large-scale mapping compared to grid-based maps, whose data size increases proportionally with the covered area. Two important techniques related to the posegraph SLAM are loop closure detection and posegraph optimization. The former technique is used for detecting loops; it matches between different portions of recorded data with high similarity. The latter is used for correcting erroneous travel data by using loops as constraints to obtain a posegraph with higher accuracy [2–9].

The  $g^2o$  (general graph optimization) solver was proposed in [3] as a powerful computational tool for posegraph

optimization. It implements several iterative methods for nonlinear least square problems such as the Gauss–Newton method and the Levenberg–Marquardt method. In addition to its computational efficiency, a major advantage of  $g^2o$  is its extensibility; new types of vertices and edges can be added by minimum amount of additional programming. One widely studied extension is robustification of the posegraph optimizer. Because of errors of loop detection, any posegraph optimization problem based on real data may include spurious loop constraints, which may cause catastrophic error in optimization results. Robust posegraph optimization is a technique to handle posegraphs including such outliers. In [4, 5] the idea of switch variables was proposed, and this idea was implemented as an extension of  $g^2o$ . This method defines a switch variable for each loop constraint. By simultaneously optimizing loop constraints and switch variables, loop constraints that do not agree with other constraints are automatically suppressed. In [6], another method based on M-estimators was proposed. This method realizes robust posegraph optimization without introducing extra variables.

One shortcoming of existing robust PGO framework is that suppression of erroneous loop constraints can only be performed on a node-pair basis; that is, even if an erroneous constraint is caused by only partial mismatch of observation data, the loop constraint must be suppressed entirely. The contribution of this paper is to propose a robust posegraph optimization method for keypoint-based posegraphs and evaluate its effectiveness using real-world data. Proximity point was proposed in the authors' previous work as a type of keypoints with several useful properties. A loop-closure detection algorithm that measures the similarity of two locations based on proximity-point matching was proposed in [10]. Moreover, a real-time detection algorithm of proximity points from 3D pointcloud and a particle-filter based self-localization method that utilizes proximity points were proposed in [11]. However, posegraph optimization based on proximity points, and its robustification, in particular, have not been discussed in the previous studies.

The organization of the rest of this paper is as follows. In Section 2, the definition and geometric characteristics of proximity points are reviewed. In Section 3, robust posegraph optimization based on proximity points is described. In Section 4, experimental results using real-



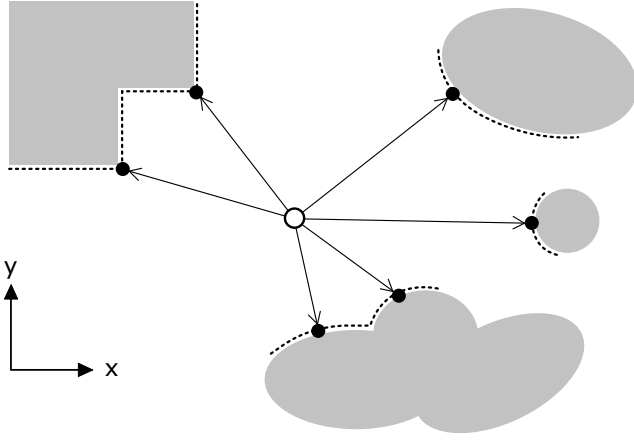


**Fig. 1.** A top-view of an environment. Multiple proximity-points (black dots) are detected on different surrounding objects (gray shapes) from a single observation point (hollow circle).

world data are presented. Concluding remarks are given in Section 5.

## 2. Definition and Geometric Properties of Proximity Points

In the following, the basic definition and geometric characteristics of proximity points are briefly reviewed. Let  $\mathcal{P} = \{\mathbf{r}_1, \dots, \mathbf{r}_N\}$  be a 3D pointcloud where each  $\mathbf{r}_i \in \mathbb{R}^3$  denotes the position of a point expressed in a 3D coordinate frame whose origin is located at the observation point. Moreover, let us define the following functions that transform a given  $\mathbf{r} = [r_x \ r_y \ r_z]^T$  into spherical coordinates.

$$\begin{aligned} d(\mathbf{r}) &= \|\mathbf{r}\|, \\ \theta(\mathbf{r}) &= \text{atan2}(r_y, r_x), \\ \phi(\mathbf{r}) &= \text{atan2}\left(r_z, \sqrt{r_x^2 + r_y^2}\right) \end{aligned}$$

As illustrated in **Fig. 1**, a proximity point is a point that is *locally nearest* to the observation point. More precisely, a point  $\mathbf{r}$  is a proximity point if the following condition is satisfied.

$$\mathbf{r} = \arg \min_{\mathbf{r}' \in \mathcal{N}(\mathbf{r})} d(\mathbf{r}') \quad (1)$$

Here,  $\mathcal{N}(\mathbf{r})$  is the set of neighboring points of  $\mathbf{r}$ , defined as follows.

$$\mathcal{N}(\mathbf{r}) = \{\mathbf{r}' \in \mathcal{P} \mid |\theta(\mathbf{r}') - \theta(\mathbf{r})| < \sigma_\theta, |\phi(\mathbf{r}') - \phi(\mathbf{r})| < \sigma_\phi\} \quad (2)$$

Here,  $\sigma_\theta$  and  $\sigma_\phi$  are parameters that determine the size of the neighborhood. Theoretically, if one could assume that the pointcloud is infinitely dense, then  $\sigma_\theta$  and  $\sigma_\phi$  could be infinitesimal; in practice, however, these parameters should be chosen carefully considering the actual spatial resolution of the pointcloud.

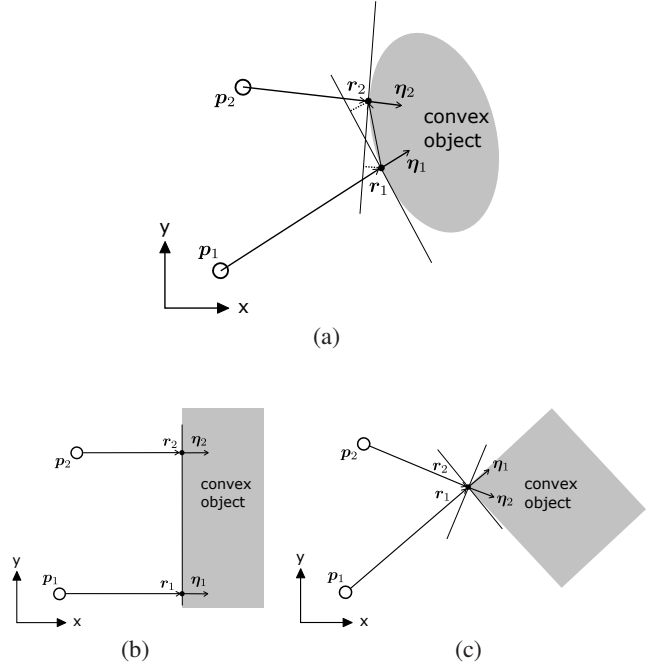


**Fig. 2.** Geometric relationship of a pair of proximity-points detected on a single convex object from different observation points.

Proximity points have some useful geometric properties that can be utilized for loop-closure detection and posegraph optimization. Consider a convex object and two different observation points whose poses in the global coordinate frame are given by  $\mathbf{x}_1 = (\mathbf{p}_1, \theta_1)$  and  $\mathbf{x}_2 = (\mathbf{p}_2, \theta_2)$ , respectively, as illustrated in **Figs. 2(a)–(c)**. Moreover, let  $\mathbf{r}_1$  and  $\mathbf{r}_2$  be two proximity points detected on the surface of the convex object from these observation points, each expressed in the local coordinate frame of the corresponding observation point. The convexity of the object implies that the following inequality generally holds.

$$\begin{aligned} \mathbf{e}(\mathbf{x}_1, \mathbf{x}_2, \mathbf{r}_1, \mathbf{r}_2) &:= \begin{bmatrix} (R(\theta_1)\boldsymbol{\eta}_1)^T((\mathbf{p}_2 + R(\theta_2)\mathbf{r}_2) - (\mathbf{p}_1 + R(\theta_1)\mathbf{r}_1)) \\ (R(\theta_2)\boldsymbol{\eta}_2)^T((\mathbf{p}_1 + R(\theta_1)\mathbf{r}_1) - (\mathbf{p}_2 + R(\theta_2)\mathbf{r}_2)) \end{bmatrix} \\ &\geq \mathbf{0} \quad \dots \quad (3) \end{aligned}$$

Here,  $\boldsymbol{\eta}_i = \mathbf{r}_i / \|\mathbf{r}_i\|$ , and the vector inequality is evaluated componentwise.

The implication of the inequality above is the following. Consider a tangent plane of the object at the proximity point  $\mathbf{r}_1$ . Then, because of the convexity of the object, the other proximity point  $\mathbf{r}_2$  must be on this tangent plane or in the opposite side of the plane from the observation point  $\mathbf{p}_1$ . The same relationship holds with the indices 1 and 2 swapped. Examples are shown in **Figs. 2(a)–(c)**. In special cases where the curvature of the object is extremely small (e.g., a wall) or extremely large (e.g., a rectangular corner of an object), these inequalities approximately hold with equality. In fact, in cases illustrated in **Figs. 2(b) and (c)**,  $\mathbf{e} = \mathbf{0}$  holds.





but the optimal value of  $s_i$  is always between 0 and 1 (it is clear from Eq. (6) that  $s_i$  outside the range  $[0, 1]$  can never be optimal). When the switch variable  $s_i$  is close to zero, the weight of the error term  $\mathbf{e}_i^T \Omega_i \mathbf{e}_i$  becomes small, and this loop constraint is effectively suppressed. The second term,  $\xi(1 - s_i)^2$ , is a penalty that must be paid for making  $s_i$  close to zero. This penalty term is needed to avoid a trivial solution with all switch variables set as zero. The value of the parameter  $\xi$ , which control the strength of this penalty term, must be determined manually.

The overall posegraph optimization problem is formulated as follows.

$$\begin{aligned} & \text{find} \quad \mathbf{x}_j (j \in \mathcal{V}), s_i (i \in \mathcal{E}_{\text{prox}}) \\ & \text{minimize} \quad \sum_{i \in \mathcal{E}_{\text{prox}}} J_{\text{prox},i} + \sum_{i \in \mathcal{E}_{\text{se2}}} J_{\text{se2},i} \dots \dots (7) \end{aligned}$$

Here,  $\mathcal{V}$  is the set of VERTEX\_PROX vertices,  $\mathcal{E}_{\text{se2}}$  is the set of EDGE\_SE2 edges, and  $\mathcal{E}_{\text{prox}}$  is the set of EDGE\_PROX edges. Note that the node poses  $\mathbf{x}_j$  and the switch variables  $s_i$  are optimized simultaneously in the single optimization problem (Eq. (7)). As a result of optimization, outlier edges that do not agree with other edges are suppressed, and node poses that minimize the total error of unsuppressed edges are computed.

As described in Section 2, the matched proximity points should satisfy the inequality (3). In other words, it is no problem if the components of  $\mathbf{e}$  take positive values. In this sense, penalizing the magnitude of  $\mathbf{e}$  as defined in Eq. (6), which essentially require  $\mathbf{e}$  to be zero, may seem inappropriate. In practice, however, many objects that appear in the environment have either very small curvature or very large curvature, in which case  $\mathbf{e}$  becomes close to zero. Moreover, it is technically difficult to handle inequality constraints in numerical optimization, especially when we do not want to modify the core optimization routine of  $g^2o$ . For this reason, we consider that cost definition (Eq. (6)) is practically acceptable.

For comparison, we also consider robust optimization based on the M-estimators: the Huber method and the Geman–McClure method. The essential idea of the M-estimator-based methods is to filter the original cost function so that the gradient of the filtered cost function saturates to a certain limit as the error becomes greater than the specified threshold. Consider a quadratic edge cost defined as  $J = \mathbf{e}^T \Omega \mathbf{e}$ . The Huber method defines the filtered cost as

$$\rho_H(J) = \begin{cases} J & \text{if } J \leq \sigma^2 \\ 2\sigma\sqrt{J} - \sigma^2 & \text{otherwise} \end{cases}, \dots \dots (8)$$

while in the Geman–McClure method, it is defined as

$$\rho_G(J) = \frac{J}{\sigma^2 + J}, \dots \dots \dots (9)$$

The profile of these functions is shown in Fig. 4 for a scalar quadratic cost  $J(x) = x^2$ . An advantage of M-estimator-based robustification is that there is no need to introduce extra decision variables. Its shortcoming is poor convergence caused by small gradient of  $\rho$  func-

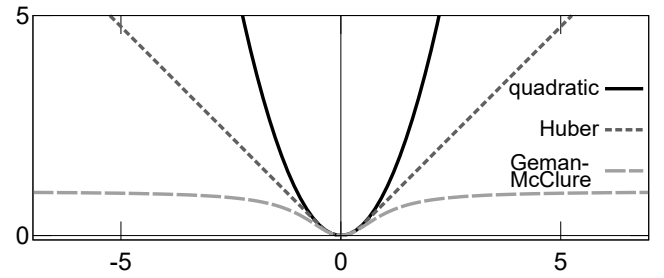


Fig. 4. Profile of cost functions: quadratic, Huber, and Geman–McClure.

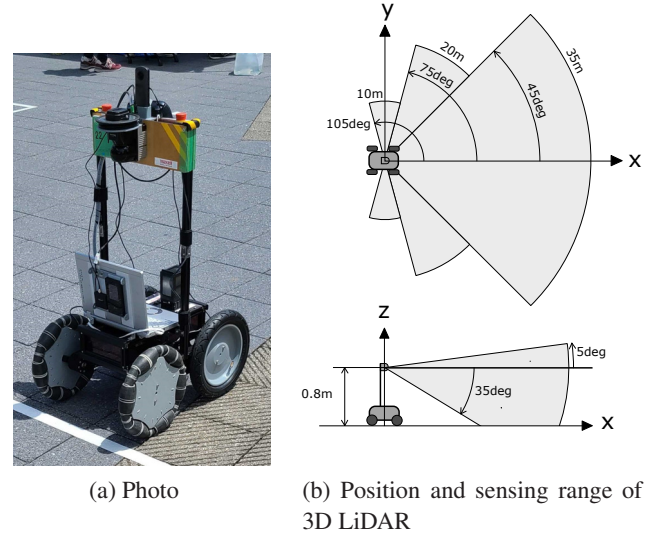


Fig. 5. Mobile robot used for data recording.

tion. Another shortcoming is that it can weaken but cannot completely nullify the influence of spurious edges.

## 4. Experimental Results

### 4.1. Experimental Setup

Experiments were conducted to evaluate the proposed robust posegraph optimization method. Fig. 5(a) shows the mobile robot Omnia3 used for data recording. It is equipped with a 3D-LiDAR (Hokuyo YVT-35LX-F0), whose installation position and sensing range are illustrated in Fig. 5(b). At a period of 500 ms, the 3D-LiDAR measures a 3D pointcloud consisting of 20,000 points, and from this pointcloud, proximity points are detected by the algorithm described in detail in [11]. An example of 3D pointcloud and proximity points detected from it is shown in Fig. 6. Statistically, the number of proximity points detected from a single set of pointcloud is 8 in average and 20 at most.

Data recording was conducted in two environments shown in Fig. 7. The first one is the course of Nakanoshima Robot Challenge 2021 Extra Challenge. Three data-recording runs were conducted, and recorded time-series were labeled NC2021-A to NC2021-C. In

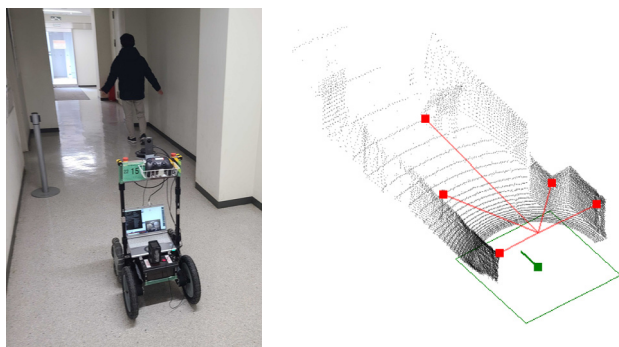
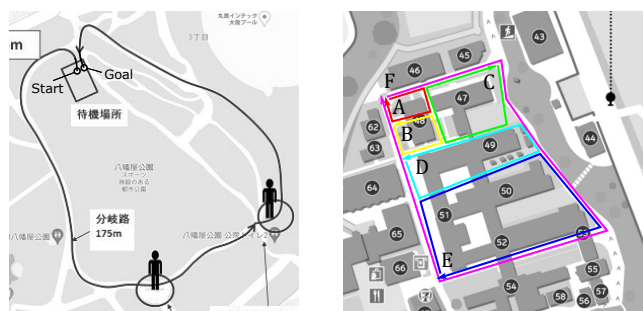


**Fig. 6.** An example scene (left), 3D pointcloud (right, black dots), and detected proximity-points (right, red square markers).



(a) Nakanoshima Robot Challenge 2021 Extra Challenge Course (excerpt from the challenge proposal)

(b) Kobe University Engineering Department building

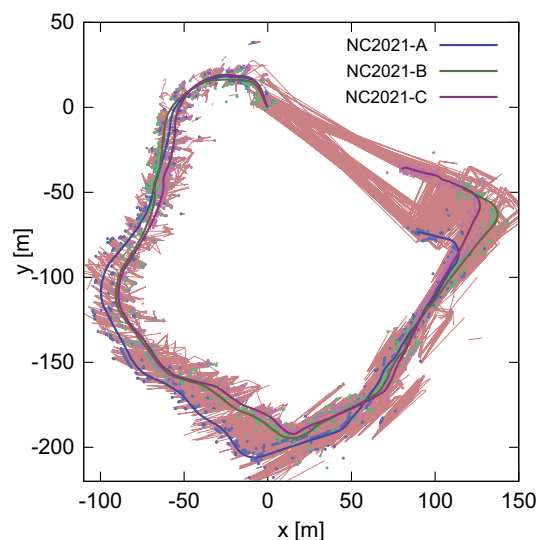
**Fig. 7.** Test environment.

each run, the mobile robot was manually operated from the starting point along the course to the goal point, and returned to the starting point. Since many pedestrians and other participating robots are in the scene, there are many sources of observation noise that cause erroneous loop-closure detection. The second environment is the Engineering Department building of Kobe University. In this environment, the mobile robot was manually operated to drive along several difference cyclic routes as shown in **Fig. 7(b)**, and the recorded data were labeled KU-A to KU-F. In the next section, we evaluate posegraph optimization results obtained by different methods in terms of the magnitude of error. Here, error refers to the value of the cost function used for optimization, and it does not refer to error from some kind of ground truth.

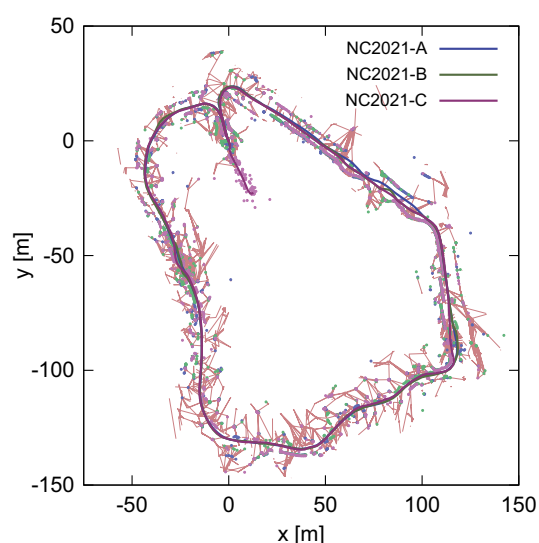
## 4.2. Posegraph Optimization Results

### 4.2.1. NC2021

**Figures 8(a) and (b)** show the posegraph of NC2021 before and after posegraph optimization. Trajectory points and proximity points that belong to different time-series (NC2021-A to NC2021-C) are depicted in different colors. We can see in **Fig. 8(a)** that large odometry error is present before optimization. Loop constraints that are de-



(a) Before



(b) After

**Fig. 8.** Before and after PGO (NC2021Ex).

tected by the loop detection method presented in [10] are depicted by pale red lines connecting matched proximity points. Loops are mainly detected between regions near the start and the goal of the same time-series, and between close regions of different time-series. **Fig. 8(b)** shows the posegraph after the application of the proposed robust PGO. We can see that error is greatly reduced. There are some remaining loop constraints shown as red lines, but they are mostly spurious loops that were suppressed thanks to robust optimization technique.

Different robust PGO methods were applied to NC2021. All compared methods could successfully reduce large odometric error that was observed before optimization. Nevertheless, small but notable differences are observed in some regions. One example of such regions is shown in the close-up images (**Figs. 9(a)–(d)**). A photo of the same region is shown in **Fig. 10**. A flower bed was located in the middle of the walkway, and in NC2021-A,

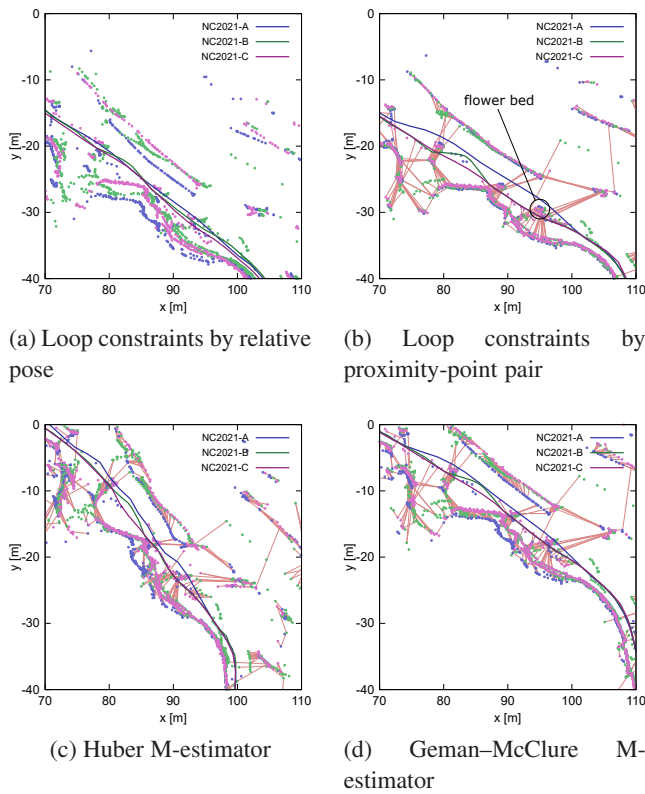


Fig. 9. Comparison of robust PGO methods.

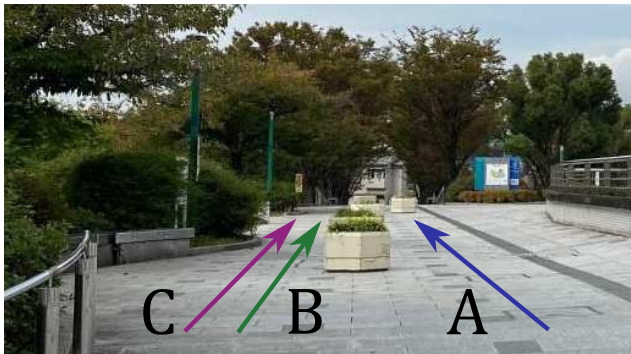


Fig. 10. Difference of routes taken around the flower bed.

the robot avoided to the right, whereas in NC2021-B and NC2021-C, it avoided to the left. This small difference of travel route caused relatively a large number of erroneous loop detections around this region. In the relative-pose-based formulation, the switch variable corresponding to loop constraints defined between nodes in this region was weakened uniformly, and there remained large error as shown in Fig. 9(a). The result of proximity-point-based formulation is shown in Fig. 9(b). Wrong proximity-point matches were weakened, while correct ones remained in effect, and as a result, a better optimization result was achieved. The results of M-estimator methods, Huber and Geman-McClure, are shown in Figs. 9(c) and (d), respectively. Here, the value of the parameter  $\sigma$  was hand-tuned to obtain the best result. Compared to the proposed

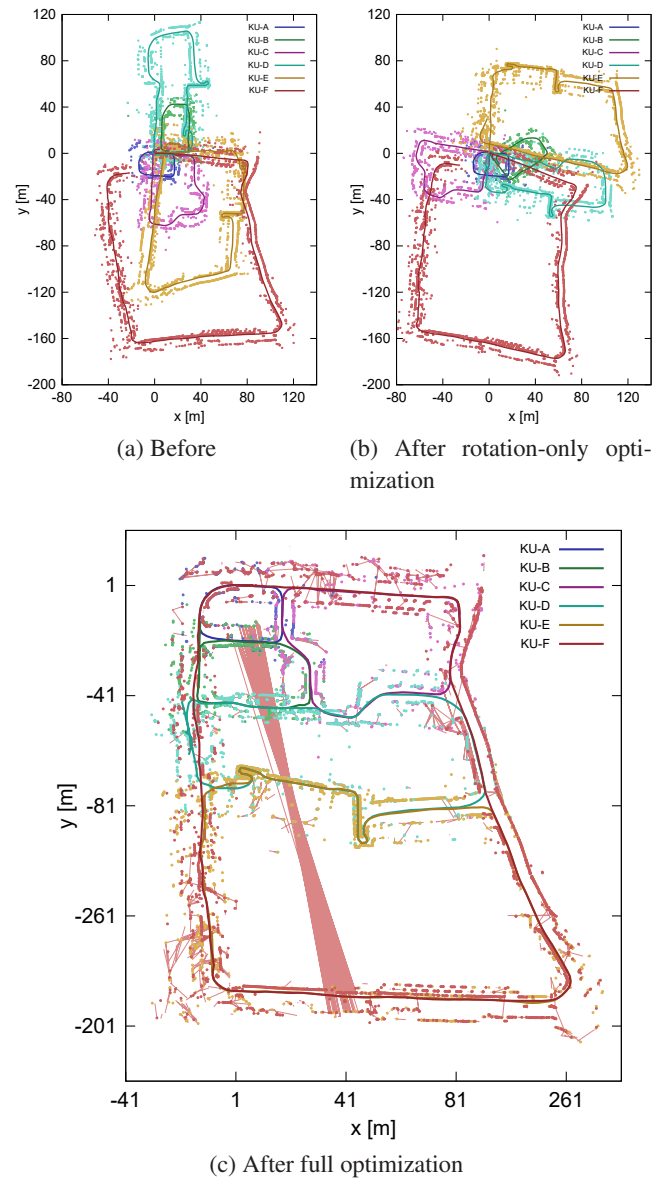


Fig. 11. Posegraph optimization results of KU.

method, average error remained large. From this result, it was found that the M-estimator method was not as good as the switch-variable method in rejecting spurious loops.

#### 4.2.2. KU

Six series of data, KU-A to KU-F were recorded and used for map construction. Loop detection were performed on every pair with overlapping routes. Figs. 11(a)–(c) show the posegraphs before and after optimization. Before optimization, the first node of each data was set to the origin and its orientation angle was zero. When PGO was directly applied to this initial configuration, it was hard to avoid converging to an erroneous local minimum. To avoid this problem, PGO was performed in two steps; in the first step, the orientation of nodes was optimized while the position was fixed, and in the second step, full optimization was computed. A set of erroneous loops were detected between KU-B and KU-F. Thanks



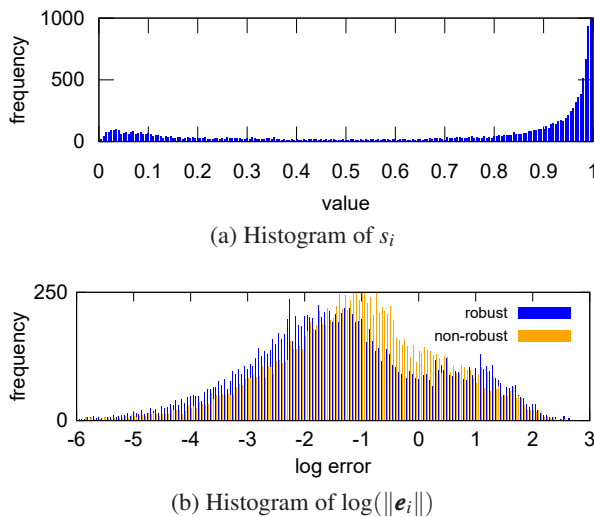


**Fig. 12.** Comparison of error distribution.

to robust optimization, these loops were suppressed and made little influence to the result.

#### 4.3. Effect of Switch Variables

For NC2021, histograms of the switch variables and the edge costs after optimization are shown in **Figs. 12(a)** and **(b)**, respectively. In **Fig. 12(b)**, the error distribution of two cases are shown: one is when the switch variables were optimized (labeled robust) and the other is when all switch variables were fixed to 1 (labeled non-robust). **Fig. 12(a)** shows that most switch variables are concentrated around the two extremes, 0 and 1, where the cluster around 1 is much larger. As shown in **Fig. 12(b)**, the error distribution without switch variable optimization (i.e., all  $s_i$  fixed to 1) has a single great peak, while the distribution with switch variable optimization shows two peaks. Here, the smaller peak on the right consists of suppressed edges, while the greater peak on the left consists of unsuppressed ones. We can see that the latter peak is shifted to the left, indicating that the average error of unsuppressed edges were reduced greatly thanks to the suppression of a smaller number of outlier edges. **Figs. 13(a)** and **(b)** show the same statistics for KU, in which similar observations can be made.

#### 4.4. Computation Cost

**Table 1** summarizes the number of iterations and total computation time of three methods: switch variables, Huber, and Geman–McClure, all based on proximity-point matching constraints. Computation was performed on a Windows computer with AMD Ryzen 9 5950X CPU with 16 cores and 32 parallel threads.

For NC2021, all three methods converged after almost the same number of iterations. Note that close-up images of optimization results are shown in **Figs. 9(b)–(d)**. The switch-variable-based method required slightly greater computation time because of the increased dimensionality of the problem. Nevertheless, the overall com-

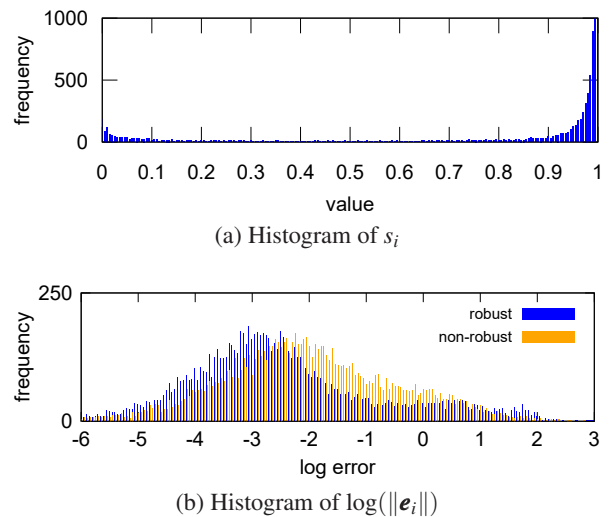


**Fig. 13.** Comparison of error distribution of KU.

**Table 1.** Number of iterations and total computation time of each method.

Method	NC2021		KU	
	# iter	Time [s]	# iter	Time [s]
Switch vars	11	2.50	36	6.06
Huber	11	1.55	–	–
Geman–McClure	10	1.44	50	5.79

putation is completed in a matter of seconds, therefore it is considered to be little problem in practice. For KU, the switch variable-based method converged successfully although a greater number of iterations was required compared to NC2021. On the other hand, the M-estimator methods performed poorly. Huber, in particular, failed to converge within 500 iterations. Geman–McClure converged, but large error remained in the output posegraph. The above results indicates the switch-variable-based method can achieve better convergence than the M-estimator methods. Although the computation time of each iteration increases, the total computation cost is reduced thanks to faster convergence.

## 5. Conclusion

This paper proposed a robust keypoint-based posegraph optimization method that can be used for large-scale mapping of outdoor environments. By assigning a switch variable to each keypoint pair, the proposed method was able to perform robust PGO in a more fine-grained manner compared to conventional methods that assign a switch variable to each node pair. One limitation of our method in the present form is that the generated posegraph retains the serial structure of recorded data it is based on. Our next goal is to extend the current framework to incremental topological map building that is capable of capturing the topological structure of the environment in the map.



## References:

- [1] C. Cadena, L. Carlone, H. Carrillo, Y. Latif, D. Scaramuzza, J. Neira, I. Reid, and J. J. Leonard, "Past, present, and future of simultaneous localization and mapping: Toward the robust-perception age," *IEEE Trans. on Robotics*, Vol.32, No.6, pp. 1309-1332, 2016. <https://doi.org/10.1109/TRO.2016.2624754>
- [2] D. M. Cole and P. M. Newman, "Using laser range data for 3d slam in outdoor environments," *IEEE Int. Conf. on Robotics and Automation (ICRA)*, pp. 1556-1563, 2006. <https://doi.org/10.1109/ROBOT.2006.1641929>
- [3] R. Kümmerle, G. Grisetti, H. Strasdat, K. Konolige, and W. Burgard, " $g^2o$ : A general framework for graph optimization," *IEEE Int. Conf. on Robotics and Automation (ICRA)*, pp. 3607-3613, 2011. <https://doi.org/10.1109/ICRA.2011.5979949>
- [4] N. Sünderhauf and P. Protzel, "Switchable constraints for robust pose graph slam," *IEEE Int. Conf. on Intelligent Robots and Systems (IROS)*, pp. 1879-1884, 2012. <https://doi.org/10.1109/IROS.2012.6385590>
- [5] N. Sünderhauf and P. Protzel, "Towards a robust back-end for pose graph slam," *IEEE Int. Conf. on Robotics and Automation (ICRA)*, pp. 1254-1261, 2012. <https://doi.org/10.1109/ICRA.2012.6224709>
- [6] P. Agarwal, G. D. Tipaldi, L. Spinello, C. Stachniss, and W. Burgard, "Robust map optimization using dynamic covariance scaling," *2013 IEEE Int. Conf. on Robotics and Automation*, pp. 62-69, 2013. <https://doi.org/10.1109/ICRA.2013.6630557>
- [7] G. Hu, K. Khosoussi, and S. Huang, "Towards a reliable slam back-end," *IEEE Int. Conf. on Intelligent Robots and Systems (IROS)*, pp. 37-43, 2013. <https://doi.org/10.1109/IROS.2013.6696329>
- [8] G. Agamennoni, P. Furgale, and R. Siegwart, "Self-tuning m-estimators," *IEEE Int. Conf. on Robotics and Automation (ICRA)*, pp. 4628-4635, 2015. <https://doi.org/10.1109/ICRA.2015.7139840>
- [9] F. Wu and G. Beltrame, "Cluster-based penalty scaling for robust pose graph optimization," *IEEE Robotics and Automation Letters*, Vol.5, No.4, pp. 6193-6200, 2020. <https://doi.org/10.1109/LRA.2020.3011394>
- [10] Y. Tazaki, Y. Miyauchi, and Y. Yokokohji, "Loop detection of outdoor environment using proximity points of 3d pointcloud," *IEEE/SICE Int. Symposium on System Integration (SII)*, pp. 411-416, 2017. <https://doi.org/10.1109/SII.2017.8279247>
- [11] Y. Tazaki and Y. Yokokohji, "Outdoor autonomous navigation utilizing proximity points of 3d pointcloud," *J. Robot. Mechatron.*, Vol.32, No.6, pp. 1183-1192, 2020. <https://doi.org/10.20965/jrm.2020.p1183>



**Name:**  
Yuichi Tazaki

**ORCID:**  
0000-0001-5087-6623

**Affiliation:**  
Associate Professor, Graduate School of Engineering, Kobe University

**Address:**

Rokkodai-cho, Nada-ku, Kobe, Hyogo 657-0013, Japan

**Brief Biographical History:**

2007-2009 Research Fellow, Japan Society for the Promotion of Science  
 2008 Received Dr.Eng. degree in Control Engineering from Tokyo Institute of Technology  
 2008 Guest Scientist, Honda Research Institute Europe  
 2009-2016 Assistant Professor, Nagoya University  
 2016- Associate Professor, Kobe University

**Main Works:**

• Autonomous vehicles, mobile robots, and humanoid robots

**Membership in Academic Societies:**

- Institute of Electrical and Electronics Engineers (IEEE)
- The Society of Instrument and Control Engineers (SICE)
- The Robotics Society of Japan (RSJ)



**Name:**  
Kotaro Wada

**Affiliation:**  
Graduate School of Engineering, Kobe University

**Address:**

Rokkodai-cho, Nada-ku, Kobe, Hyogo 657-0013, Japan

**Brief Biographical History:**

2023 Received M.S. degree in Engineering from Kobe University

**Main Works:**

- Map generation of mobile robots



**Name:**  
Hikaru Nagano

**ORCID:**  
0000-0001-5230-6288

**Affiliation:**  
Graduate School of Engineering, Kobe University

**Address:**

Rokkodai-cho, Nada-ku, Kobe, Hyogo 657-0013, Japan

**Brief Biographical History:**

2010 Received B.S. degree in Engineering from Nagoya University  
 2012 Received M.S. degree in Engineering from Nagoya University  
 2015 Received Ph.D. degree in Engineering from Nagoya University  
 2015-2018 Assistant Professor, Tohoku University  
 2018- Assistant Professor, Graduate School of Engineering, Kobe University

**Main Works:**

- Human haptic perception and human-machine interfaces

**Name:**

Yasuyoshi Yokokohji

**ORCID:**

0000-0001-8869-7102

**Affiliation:**

Professor, Graduate School of Engineering,  
Kobe University

**Address:**

Rokkodai-cho, Nada-ku, Kobe, Hyogo 657-0013, Japan

**Brief Biographical History:**

1984 Received B.S. degree in Precision Engineering from Kyoto University

1986 Received M.S. degree in Precision Engineering from Kyoto University

1988-1989 Research Associate, Automation Research Laboratory, Kyoto University

1989-1992 Research Associate, Division of Applied Systems Science, Faculty of Engineering, Kyoto University

1991 Received Ph.D. degree in Mechanical Engineering from Kyoto University

1992-2005 Associate Professor, Department of Mechanical Engineering, Kyoto University

1994-1996 Visiting Research Scholar, Robotics Institute, Carnegie Mellon University

2005-2009 Associate Professor, Department of Mechanical Engineering and Science, Graduate School of Engineering, Kyoto University

2009- Professor, Department of Mechanical Engineering, Graduate School of Engineering, Kobe University

**Main Works:**

- Robotics and virtual reality including teleoperation systems, robot hands, and haptic interfaces

**Membership in Academic Societies:**

- The Robotics Society of Japan (RSJ), Fellow
  - The Japan Society of Mechanical Engineers (JSME)
  - The Society of Instrument and Control Engineers (SICE)
  - The Institute of Systems, Control and Information Engineers (ISCIE)
  - The Virtual Reality Society of Japan (VRSJ)
  - Institute of Electrical and Electronics Engineers (IEEE), Senior Member
  - Industrial Robotics Competition Committee, World Robot Summit, Chairperson
-